Phonon dispersion curves in an argon single crystal at high pressure by inelastic x-ray scattering

F. Occelli,[1] M. Krisch,[2] P. Loubeyre,[1] F. Sette,[2] R. Le Toullec,[1,3] C. Masciovecchio,[2] and J.-P. Rueff[2]
[1]*DIF/DPTA/SPMC, CEA 91680 Bruyères-le-Châtel, France*
[2]*European Synchrotron Radiation Facility, BP 220, F-38043 Grenoble Cedex, France*
[3]*Université Pierre et Marie Curie, Physique des Milieux Condensés, T13, E4, B77, 4 Place Jussieu, 75252 Paris Cedex 05, France*
(Received 7 December 2000; published 23 May 2001)

The phonon dispersion of fcc argon under high pressure to 20 GPa has been measured along the (100) direction by inelastic x-ray scattering. First, this shows a novel possibility to investigate the single crystal dynamical properties under very high pressure in a diamond anvil cell. Second, the comparison between experiment and phonon calculations, using pair potentials (either the pure two-body potential or an effective pair potential) and a Slater-Kirkwood form for the three-body interaction, clearly demonstrates that phonon energies can be strongly influenced under high pressure by the nonadditive part of the interaction.

DOI: 10.1103/PhysRevB.63.224306 PACS number(s): 62.50.+p, 63.20.−e, 83.85.Hf, 34.20.Cf

I. INTRODUCTION

The determination of the phonon spectra in a material under pressure is essential for understanding the effects of density on the mechanical stability, the phase transition mechanisms, the material strength, the transport properties, and the interatomic interactions. In fact, coupled with the structural determination, it gives a complete atomic-scale understanding of the thermodynamics of the system.

Up to now, phonon measurements have been performed by inelastic neutron scattering, on mm^3 size single-crystals in order to have reasonable signals. Remarkably, developments in neutron high-pressure techniques have recently allowed the determination of the phonon dispersion curve up to 10 GPa in germanium[1] and iron.[2] Inelastic x-ray scattering (IXS) with very high-energy resolution and the high flux of a third generation synchrotron source is another spectroscopic technique potentially suited to extend the phonon spectra determination on single crystals compressed up to the 100 GPa range in a diamond anvil cell. Indeed, the direction-averaged longitudinal acoustic-phonon dispersion in CdTe has already been measured at 7.5 GPa by IXS (Ref. 3) on a polycrystalline sample of around $10^{-3}\,mm^3$.

The first aim of the present work is to show, as a proof of principle, that the phonon branches can be accurately measured by IXS on a single crystal compressed in a diamond anvil cell. The other aim is to probe the effect of the nonadditivity of the interaction on the phonon dispersion curves at high pressure. The influence of the triple-dipole interaction was established some 30 years ago by Barker *et al.*[4] The increasing importance of nonadditive exchange interactions with pressure will also certainly influence the phonon dispersion curves, probably more drastically than the triple-dipole forces at ambient pressure. This is certainly an important question because non-additive embedded-atom potentials are currently used to calculate the properties of heterogeneous systems at high density[5] or to calculate large scale structures and phenomena at high pressure,that would require otherwise too much computational time by *ab initio* methods.[6]

In this context, measurements are reported on a single-crystal of argon. Argon being a low-Z system, it implies that what has been measured here can certainly be observed on higher Z crystals on much smaller samples (hence much higher pressures). Also, the interaction in solid argon has been studied extensively and is well represented by the sum of pair interactions between argon atoms[7] with the addition of nonadditive contributions.[8] Thereof, the effect of the nonadditivity of the forces can be addressed.

The IXS technique for single crystal and experimental details are presented in Sec. II. The data are presented in Sec. III. Section IV discusses the theoretical models and the confrontation with experiment. The influence of non additive interactions to the phonon branch is discussed in Sec. IV B. Our conclusions are summarized in Sec. V.

II. EXPERIMENTAL DETAILS

The single crystal of Ar was obtained by the slow growth of a single germ at the solidification pressure of argon (1.35 GPa at 298 K). A volume chamber of about 300 μm diameter and 100 μm thickness was obtained by using large diamond anvils with 800 μm flat culets. The membrane diamond anvils cell with a large x-ray aperture was loaded in a high pressure vessel under 100 MPa.[9] Pressure was measured with the ruby luminescence gauge.[10] The orientation matrix of the single crystal of argon was determined before hand with the single crystal energy dispersive technique.[11]

The experiment was carried out at the inelastic x-ray scattering beamline I (ID 16) at the European Synchrotron radiation facility in Grenoble (France). The high resolution monochromator-analyzer setup was operated utilizing the Si(999) reflection order, which provides an overall energy resolution of 3 meV (at 17794 eV) with an incident photon flux of 3×10^9 photons/s.[12–14] The scattered photons are energy analyzed by a Rowland circle five-crystal spectrometer. The energy-analyzed photons are detected by a Peltier-cooled silicon diode detector which has an intrinsic energy resolution of 400 eV. The dark counts due to electronic and environmental noise amounts to about 0.2 counts/min. The momentum transfer is selected by rotating the spectrometer around a vertical axis passing through the scattering sample in the horizontal plane. Since there are five independent

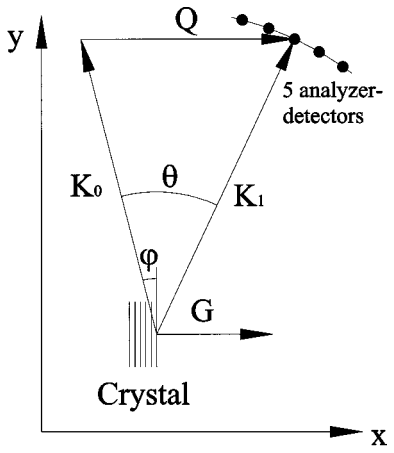

FIG. 1. Schematic view of the experimental setup.

analyzer-detector systems, spectra at five different momentum transfers can be recorded simultaneously. Their separation is energy dependent and for the Si(999) reflection, utilized in the present experiment, this separation amounts to $2.5\,\mathrm{nm}^{-1}$. The energy scans are performed by varying the monochromator temperature while the analyzer temperature is kept fixed. Conversion from the temperature scale to the energy scale is accomplished by the following relation: $\Delta E/E=\alpha\Delta T$, where $\alpha=2.56\times10^{-6}\,\mathrm{K}^{-1}$ is the linear thermal expansion coefficient of silicon at room temperature. The validity of this conversion has been checked by comparing the experimentally determined diamond dispersion curve for longitudinal acoustic photons with well established inelastic neutron scattering results. In order to avoid parasitic scattering from the stainless steel high pressure gasket, the focused beam of 270(horizontal)$\times$130(vertical) $\mu\mathrm{m}^2$ full width at half maximum (FWHM) was further reduced to $100\times140\,\mu\mathrm{m}^2$. The crystal was aligned along the (100) direction in the horizontal scattering plane of the spectrometer. The correct size of the momentum transfer and its direction can be derived from straightforward trigonometric considerations as seen in Fig. 1. The horizontal scattering plane is defined by the two cartesian axes x and y where the reciprocal lattice vector $\boldsymbol{G}$ (here 100) is directed along x. With this convention $\boldsymbol{G}$, the incident photon wave vector $\boldsymbol{K}_0$, and the scattered wave vector $\boldsymbol{K}_1$ are given by

$$\boldsymbol{G}=(G,0,0),$$

$$\boldsymbol{K}_0=(-K_0\sin\varphi,K_0\cos\varphi,0), \tag{1}$$

$$\boldsymbol{K}_1=[K_1\sin(\theta-\varphi),K_1\cos(\theta-\varphi),0],$$

where φ is the angle between $\boldsymbol{K}_0$ and the y axis (glancing angle of incidence onto the lattice planes corresponding to the reciprocal vector $\boldsymbol{G}$) and θ is the scattering angle, defined as the angle between $\boldsymbol{K}_0$ and $\boldsymbol{K}_1$. Assuming $K_0=K_1$, the momentum transfer is given by

$$\boldsymbol{Q}=\boldsymbol{K}_1-\boldsymbol{K}_0,$$

$$\boldsymbol{Q}=K_0[\sin(\theta-\varphi)+\sin\varphi,\cos(\theta-\varphi)-\cos\varphi,0] \tag{2}$$

with its modulus :

$$Q=K_0\sqrt{2(1-\cos\theta)}. \tag{3}$$

Only if $\varphi=\theta/2$, the momentum transfer is along G. This condition was set for the third analyzer detector. In the general case, the angular deviation δ of $\boldsymbol{Q}$ with respect to $\boldsymbol{G}$ is determined using the above relations

$$\delta=\cos^{-1}\left(\frac{Q_x}{Q}\right). \tag{4}$$

The above described procedure was used to calculate the correct momentum transfer values. The angular deviation of the momentum transfer with respect to the [100] direction amounts to 3° in the worst case. The Q resolution ΔQ is defined by fixed slits in front of the analyzer crystal, was $\pm0.15\,\mathrm{nm}^{-1}$.

The selection rule[15], $\boldsymbol{Q}\cdot\boldsymbol{e}_{j\boldsymbol{K}}\neq0$, where $\boldsymbol{e}_j$ is the polarization vector of the phonon, prevents the observation of the transverse phonon for a momentum transfer limited to the first Brillouin zone, because then $\boldsymbol{Q}=\boldsymbol{K}$ and so $\boldsymbol{K}\cdot\boldsymbol{e}_{j\boldsymbol{K}}=0$. However, for momentum transfer $\boldsymbol{Q}$ outside the first Brillouin zone, $\boldsymbol{Q}$ can be written as $\boldsymbol{Q}=\boldsymbol{K}+\boldsymbol{G}$, where $\boldsymbol{G}$ is the first nearest reciprocal lattice vector and $\boldsymbol{K}$ is in the first Brillouin zone. In that case, if $\boldsymbol{Q}$ is nonparallel to $\boldsymbol{G}$, $\boldsymbol{Q}\cdot\boldsymbol{e}_{j\boldsymbol{K}}$ is nonzero for transverse phonon, and even if $\boldsymbol{Q}$ differs by a few degrees only from the $\boldsymbol{G}$ direction, transverse mode along the $\boldsymbol{G}$ direction are measured with a good approximation.

III. EXPERIMENTAL DATA

Figure 2 shows typical IXS scans at 3.1 GPa. At a given momentum transfer, the count rates with error bars, is plotted versus the energy of the analyzer. They result from a sum of 11 (16) individual scans (the integration time of a scan was 3 h with 60 sec integration time per point). When Q is in the first Brillouin zone (BZ), as in Fig. 2(a), the Rayleigh line and an inelastic peak corresponding to a longitudinal phonon are measured. When Q is in the second BZ, longitudinal and transverse phonon peaks can be observed, as seen in Fig. 2(b).

Keeping the quality of the single crystal is certainly a central issue to be able to collect good data. The pressure on the sample was increased too rapidly from 3.1 to 20 GPa and the mosaic spread of the crystal, increased from 0.1° at 3.1 GPa, to around 5° at 20 GPa. Consequently, the IXS scan is much deteriorated as seen in Fig. 2(c). The energy position of the excitation were determined fitting the spectra with a model function composed of Lorentzians for the inelastic signal (1 or 2 depending on whether a transverse mode was observed) and a Lorentzian for the central peak. This model function was convoluted with the experimentally determined energy resolution function. The fit to the experimental data was performed by standard χ^2 minimization under the condition that the detailed balance between Stokes and anti-Stokes excitations is fulfilled.

The (100) dispersion curve constructed from measurements at various Q transfer is shown in Fig. 3 and the data

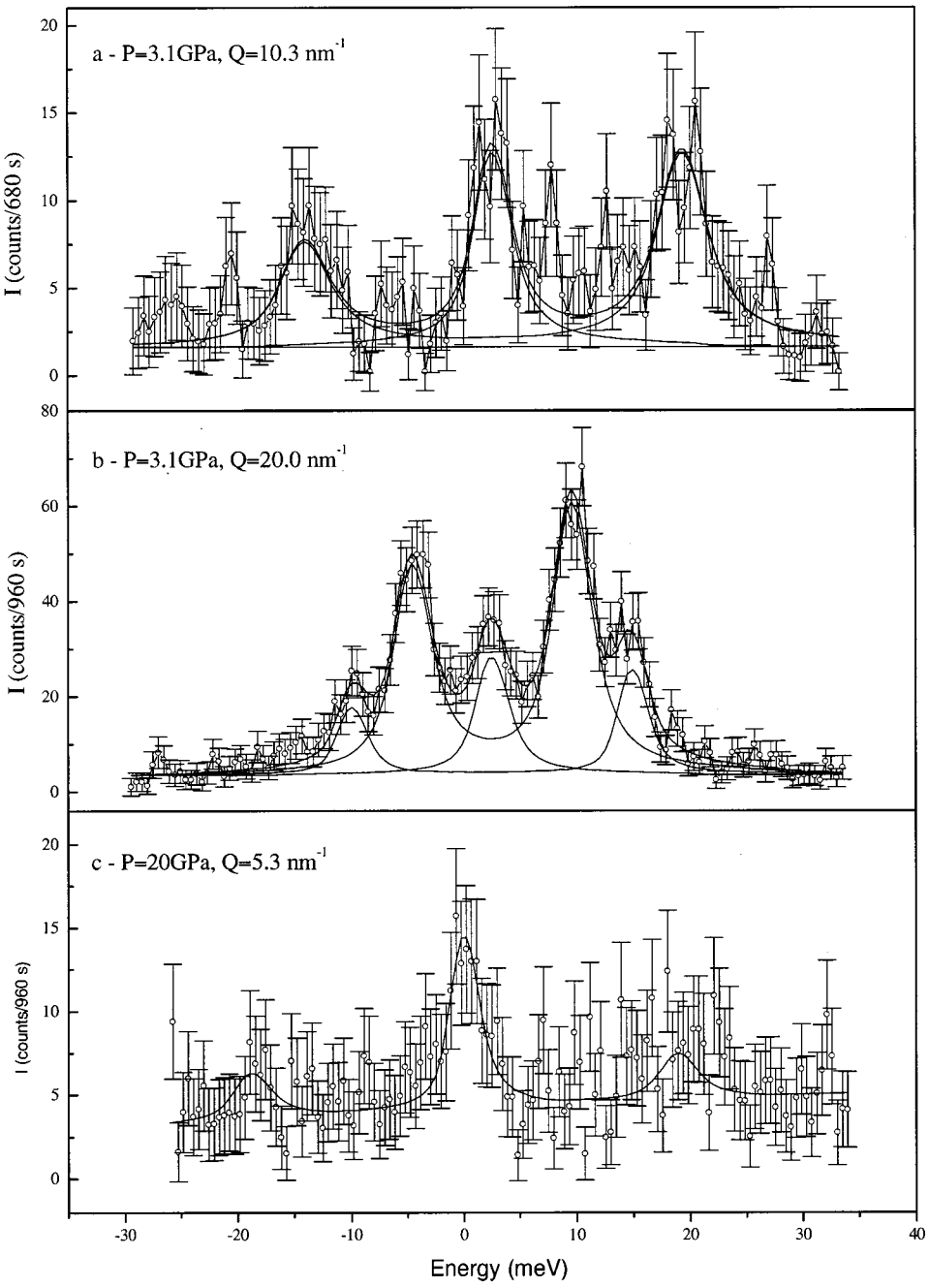

FIG. 2. Raw spectra obtained on ID 16 at the ESRF : the upper spectrum corresponds to a fixed momentum transfer belonging to the first Brillouin zone; one can distinguish on it the Stokes and anti-Stokes peaks coming from longitudinal phonons. The middle spectrum corresponds to a fixed momentum transfer in the second Brillouin zone; four peaks can be seen and correspond to longitudinal and transverse phonons. The lower spectrum corresponds to the crystal at 20 GPa with a 5% mosaicity.

reported in Table I. The $\Omega(Q)$ data are fitted like standard acoustic branch with a sine function by fixing the maximum of the dispersion curve at the BZ edge ($Q_{BZ}=12.97\,nm^{-1}$, as measured from the single crystal diffraction data under the same thermodynamical conditions). That gives a longitudinal acoustic speed of sound, $c_{LA}=3250\pm50$ m/s and a transverse acoustic speed of sound, $c_{TA}=2000\pm50$ m/s. This determination is in very good agreement with the Brilloin scattering data of Grimsditch *et al.*[16] as seen in Table II. An alternative fit, leaving $Q_{BZ}(100)$ as a free parameter, yields a slightly lower speed of sound of 3200 m/s, the difference being within the error bar. The elastic constants $C_{11}=\rho c_{LA}^2$ and $C_{44}=\rho c_{TA}^2$ are straightforwardly calculated. Using the bulk modulus (derived from the experimental EOS), the value of C_{12} can also be calculated, as reported in Table II. Thereof the Cauchy relation that quantifies the deviation of the interactions of the system from additivity is estimated. Its value, 0.4, indicates that non additive interactions certainly are significant at 3 GPa, confirming the conclusion of the Brillouin scattering study of Grimsditch *et al.*[16]

IV. PHONON CALCULATIONS

A. The pair potential approach

The phonon dispersion curve of an fcc cubic crystal can be straightforwardly calculated if a pair potential is assumed to model the interactions between the atoms. In the quasi-

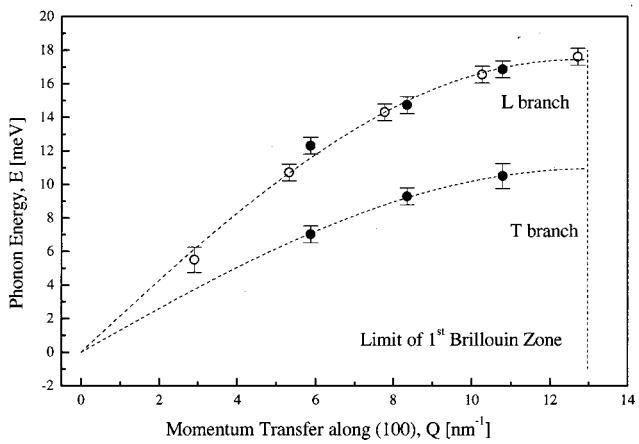

FIG. 3. Phonon dispersion curve of Ar along the (100) direction at 3.1 GPa. The symbols are ○: IXS longitudinal data obtained in the first Brillouin zone, ●: IXS longitudinal and transverse data obtained in the second Brillouin zone and reduced in the first Brillouin zone, - - -: sinus fit to IXS data.

harmonic approximation, the three acoustic frequencies $\nu_i(\boldsymbol{q})$ corresponding to the wave vector $\boldsymbol{q}$ are determined by the eigenvalue equation

$$4\pi^2 m \nu_i(\boldsymbol{q})^2 u_\alpha^i(\boldsymbol{q}) = \sum_{\beta=1}^{3} \mathcal{D}_{\alpha\beta}(\boldsymbol{q}) u_\beta^i(\boldsymbol{q}). \tag{5}$$

To take into account anharmonic contributions, that are not negligible in solid argon under the thermodynamic conditions of the confrontation experiment theory presented below,[8] the force constant used to calculate the dynamical matrix can be self-consistently averaged over the position of the atoms undergoing the thermal motion. This is the self-consistent harmonic theory that can also be corrected for cubic anharmonic terms.[18] The alternative approach, used in the present study, is to average the force constants over the motion of the atoms during a molecular dynamic simulation. The simulation was performed on a system of 2048 atoms, initially placed on the sites of an fcc lattice with periodic boundary conditions in the (N,V,E) microcanonical ensemble. The constancy of the energy E was checked every 10 time steps. The time step was set to 5×10^{-14} s, and was estimated as 1×10^{-2} of the Einstein cage period of an atom. The pressure was calculated with the virial theorem.[19] The dynamical matrix element

TABLE I. Results of our measurements. The momentum transfers (Q) are in nm^{-1} and the energies are in meV. The limit of the first Brillouin zone is 12.968 nm^{-1}; $Q^{(1)}$ is the reduced value of the momentum transfer in the first BZ. ΔE_L and ΔE_T are the error bars.

First BZ					
Q		E_L	ΔE_L		
2.91		5.5	0.75		
5.33		10.7	0.5		
7.78		14.3	0.5		
10.27		16.5	0.5		
12.72		17.6	0.5		
Second BZ					
Q	$Q^{(1)}$	E_L	ΔE_L	E_T	ΔE_T
15.14	10.80	16.8	0.75	10.5	0.5
17.58	8.36	14.7	0.5	9.3	0.5
20.06	5.88	12.3	0.5	7.0	0.5

$$\mathcal{D}_{\alpha\beta}(\boldsymbol{k}) = 2\sum_{\boldsymbol{r}_j} \left[x_\alpha^j x_\beta^j \left(\frac{1}{r^2}\frac{\partial^2 U(r)}{\partial r^2} - \frac{1}{r^3}\frac{\partial U(r)}{\partial r} \right)\Bigg|_{r=r_j} + \delta_{\alpha\beta}\left(\frac{1}{r}\frac{\partial U(r)}{\partial r} \right)\Bigg|_{r=r_j} \right] \sin^2\left(\frac{1}{2}\boldsymbol{k}\cdot\boldsymbol{r}_j \right) \tag{6}$$

was calculated at each time step. With Eq. (5) the TA and LA phonon frequencies along the (100) direction were obtained for 25 values of $|\boldsymbol{q}|$ equally spaced in the first Brillouin zone. The simulated phonon frequencies correspond then to the time average of the longitudinal and transverse frequencies. This method should adequately take into account the anharmonic contributions.

Two pair potentials were used in these simulations. First, the state of the art pair potential of argon, dubbed HFDID1, which is constrained by a large set of pair potential properties.[7] Second, a pair potential, dubbed exp-6, inverted from Hugoniot measurements which should reproduce better the properties of dense argon[17] because it includes the many-body contributions averaged in its two-body form. In Fig. 4, the $P(V)$ curves calculated with the two pair potentials are compared to the x-ray data.[17] The calculation with the HFDID1 potential is in very good agreement with experiment below 10 GPa but exponentially diverges above as expected due to the increasing importance of many-body

TABLE II. Comparison between our measurements and the Brillouin scattering data (Ref. 16). Sound speeds are in m/s and elastic constants in GPa. $C_{11}=\rho\sqrt{c_L}$, $C_{44}=\rho\sqrt{c_T}$, and $C_{12}=(3B-C_{11})/2$ is calculated via the bulk modulus $B=16.0$ GPa derived from the EOS published by Ross *et al.* (Ref. 17). The density $\rho=2.398$ g/cm^3 comes from direct measurement of the cell parameter of our sample. $A=2C_{44}/(C_{11}-C_{12})$ and $\delta=(C_{44}-C_{12}+2P)/C_{12}$ are the anisotropy factor and the Cauchy relation, respectively.

	c_L	c_T	C_{11}	C_{12}	C_{44}	A	δ
This work	3250±50	2000±50	25.3±0.8	11.4±0.4	9.6±0.5	1.4±0.2	0.4±0.1
Grimditch *et al.* (Ref. 16)	3160±50	1990±50	24	12.3	9.5	1.62	0.27

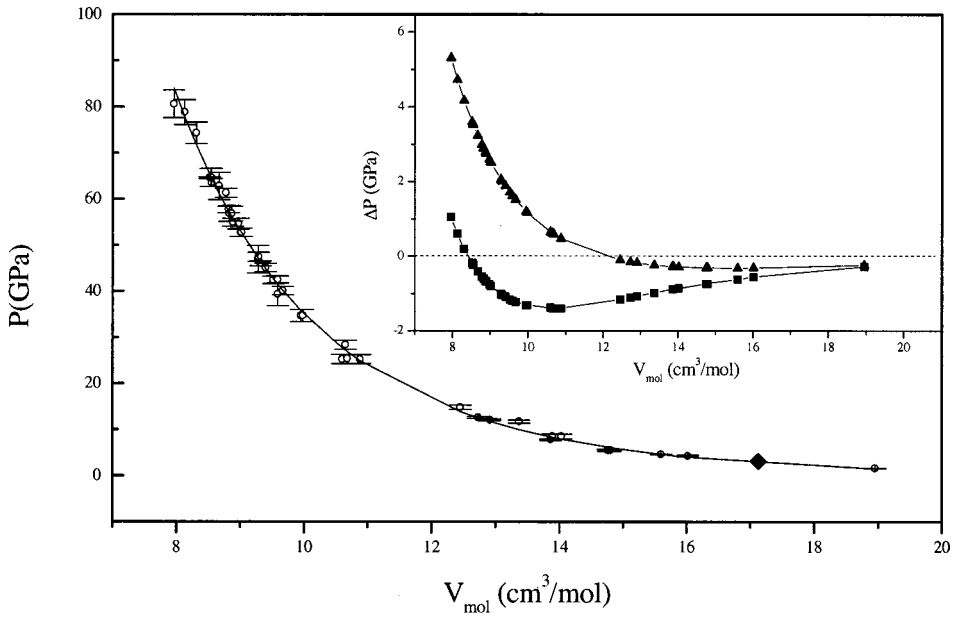

FIG. 4. Equation of state of argon, comparison between x-ray data (Ref. 17) and simulations with two pair potentials, the exp-6 (Ref. 17) one and the HFDID1 one (Ref. 7). Main figure: the dots represent the x-ray data with error bars and the line is the Vinet fit (Ref. 22): $P=3K_0x^{-2}(1-x)\exp[3/2(K_0'-1)(1-x)]$ with $x=(V/V_0)^{1/3}$ and with parameters $B_0=1.157$ GPa, $B_0'=7.950$, and $V_0=26.858\,\mathrm{cm}^3/\mathrm{mol}$. ♦ is the x-ray determination of our sample at 3.1 GPa. Inset: difference between the measured and calculated $P(V)$. The symbols are ▲ $P_{\mathrm{Vinet}}-P_{\mathrm{HFDID1}}$; ■ $P_{\mathrm{Vinet}}-P_{\mathrm{exp-6}}$.

forces.[8] On the other hand, the exp-6 potential gives a good overall agreement up to 80 GPa, that is for the pressure range over which this effective pair potential has been adjusted with dynamical measurements. Therefore, one can say that within experimental error bars, both pair potentials satisfactorily reproduce the equation of state of argon below 10 GPa with no clear evidence of the many-body contribution. However, in the previous paragraph, we have shown through the Cauchy relation that non central forces are not negligible at 3.1 GPa. It is interesting to see below what is the effect of such forces on the phonon branch.

The phonon calculation was first performed at ambient pressure and 4.2 K, where very accurate volume and phonon dispersion data have been measured some 30 years ago. The measured lattice constant is $a=5.311$ Å and the INS phonon dispersion data of Batcheler *et al.*[20] are reported in Fig. 5. With the HFDID1 potential, the transverse branch is perfectly reproduced and the longitudinal is reproduced within error bars. The exp-6 gives a less satisfactory agreement, especially for the transverse branch. Therefore at ambient pressure one may say that nonadditive interactions have a minor contribution on the equilibrium volume and dynamics of solid argon. It is interesting to note that at ambient pressure, although nonadditive interactions have minor effects on the volume and the phonon frequencies, it was recently shown that they are responsible for the stability of the fcc structure.[21]

In Fig. 6, the IXS (100) phonon data at 3.1 GPa are compared to the simulated phonon branch at the same volume (experimental cell parameter $a=4.845$ Å). The HFDID1 pair potential gives a very good agreement for the longitudinal branch but gives too high transverse frequencies by 10%. On the other hand, the exp-6 potential gives a good agreement with the transverse branch but underestimates the longitudinal branch by 7%. Because of the effect of many-body interactions, the pure pair potential cannot perfectly reproduce the properties of solid argon at 3.1 GPa, giving a small deviation on the EOS (2.8 GPa simulated instead of 3.1 GPa at $a=4.845$ Å) and a more significant deviation on the transverse phonon energy. If an effective exp-6 pair potential is used, a reasonable agreement is achieved on the EOS (2.8 GPa simulated) but here again, it is not possible to reproduce correctly the phonons dispersion curves. This is in a more detailed form what the Cauchy relation is telling us. In the next section, we will try to estimate the many-body corrections to the phonon frequencies.

B. The many-body contribution

The effect of the triple-dipole forces on the phonon branch of argon has been established by Barker *et al.*[4] In particular, it was shown that this three-body dispersion force has practically no effect on the transverse phonon branch

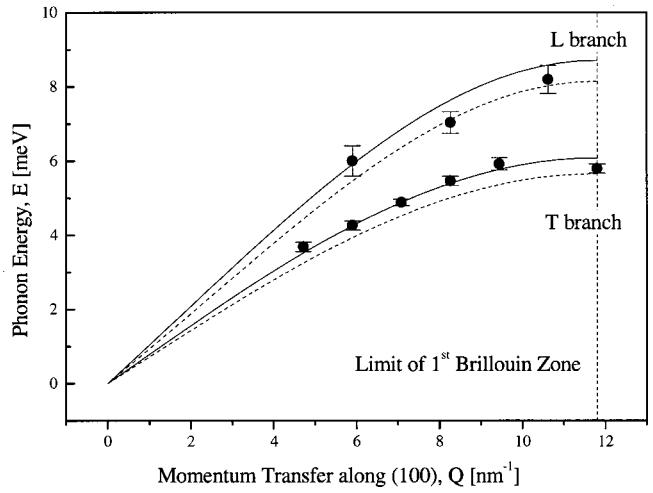

FIG. 5. Phonon dispersion of Ar at $T=4.2$ K and ambient pressure. Comparison between calculated phonon branches along (100) and INS measurements (Ref. 20). The symbols are ●: INS data, —: calculations using the HFDID1 potential (Ref. 7) - - - : calculations using exp-6 potential (Ref. 17).

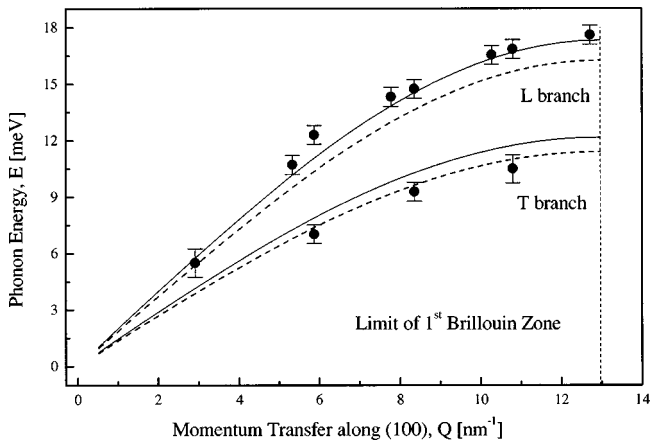

FIG. 6. Comparison between calculated phonon branches along (100) and the IXS data. The symbols are ●: IXS measurements, ···: sinus fits to IXS data, —: calculations using the HFDID1 potential (Ref. 7), - - -: calculations using the exp-6 potential (Ref. 17).

whereas it increases the longitudinal branch. This cannot explain the discrepancy discussed in the previous paragraph between the calculation with the HFDID1 potential and the IXS data at 3.1 GPa because there, the difference is observed for the transverse branch. But, nonadditive exchange interactions are becoming increasingly important under pressure and so they could have a larger contribution on the transverse branch than on the longitudinal branch.

We have tried to estimate the contribution of the nonadditive exchange interaction. For this, we have used the method of homogeneous deformations proposed by Zucker and Chell[23] and used the notations of Bell and Zucker.[18] We assumed a reasonable many-body interaction at 3.1 GPa, namely, the Slater-Kirkwood form with parameters derived from high-pressure experiments by Loubeyre[8] [see Eq. (7) and Fig. 7]. The first exponential term represents the exchange three-body interaction and the other term the triple-dipole term.

$$W=\{-A\exp[-\alpha(r_1+r_2+r_3)]+C(r_1r_2r_3)^{-3}\}\times(1+3\cos\theta_1\cos\theta_2\cos\theta_3) \tag{7}$$

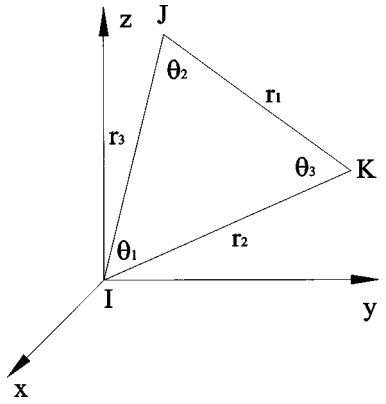

FIG. 7. Geometry of the system of three particles *I*, *J*, and *K*.

with parameters $A=2\,929\,433.3\times e$, $\alpha=1.650\,\text{Å}^{-1}$, $C=3770\times e$, $e=143.224\,\text{K}$.

In writing $d=a/2$ where a is the cell parameter $r_1^2=Id^2$, $r_2^2=Jd^2$, and $r_3^2=Kd^2$, Eq. (7) can be written in the more convenient reduced form

$$\mathcal{W}=\left(-\frac{Ad^3}{C}\exp[-\alpha d(\sqrt{I}+\sqrt{J}+\sqrt{K})]+(IJK)^{-3/2}\right)\times\left(1+\frac{3}{8IJK}(I+J-K)(I-J+K)(-I+J+K)\right). \tag{8}$$

Following Zucker, the three-body components in C_{11} and C_{44} can be calculated as

$$vC_{11}^{(3)}=sZ^{(3)}[T_2+2T_3]d^{-(p+3)},$$

$$vC_{44}^{(3)}=sZ^{(3)}[T_4+2T_6]d^{-(p+3)} \tag{9}$$

with

$$T_1=\frac{d^{p+5}}{2}\sum_{\boldsymbol{J}\neq\boldsymbol{K}}J_x^2D_J\mathcal{W},$$

$$T_2=\frac{d^{p+7}}{2}\sum_{\boldsymbol{J}\neq\boldsymbol{K}}J_x^4D_J^2\mathcal{W},$$

$$T_3=\frac{d^{p+7}}{2}\sum_{\boldsymbol{J}\neq\boldsymbol{K}}J_x^2K_x^2D_JD_K\mathcal{W},$$

$$T_4=\frac{d^{p+7}}{2}\sum_{\boldsymbol{J}\neq\boldsymbol{K}}J_x^2J_y^2D_J^2\mathcal{W},$$

$$T_5=\frac{d^{p+7}}{2}\sum_{\boldsymbol{J}\neq\boldsymbol{K}}J_x^2K_y^2D_JD_K\mathcal{W},$$

$$T_6=\frac{d^{p+7}}{2}\sum_{\boldsymbol{J}\neq\boldsymbol{K}}J_xJ_yK_xK_yD_JD_K\mathcal{W},$$

where $v=2d^3$, $D_J=(1/J)(\partial/\partial J)$, $D_K=(1/K)(\partial/\partial K)$, $p=6$, $s=1$, and $Z^{(3)}=7.75\times10^{-3}$ S.I.

The calculation was checked by comparing the three-body correction to the bulk modulus either calculated as a combination of T_i sums or directly as the derivative of the three body energy, i.e., in comparing $-11T_1$ with $T_2+2T_3+2T_4+4T_5$, we make sure that the corrections to the elastic constants we calculate verify the relation $B^{(3)}=(C_{11}^{(3)}+2C_{12}^{(3)}+P^{(3)})/3$ where $B^{(3)}$ is the three-body forces correction of the bulk modulus and $P^{(3)}=-\partial E_{\text{tot}}^{(3)}/\partial V$. The corrections to C_{11} and C_{44} at different pressures are reported in Table III. They indicate a larger correction on the longitudi-

TABLE III. Calculation of the three-body forces corrections to the elastic constants in the simple case of Axilrod-Teller interaction. P is the estimated pressure with the EOS of argon. ρ is in g/cm^3 and the pressurelike quantities are in GPa. The T_i are the lattice sums used in the Zucker formalism (Ref. 23).

ρ	P	$C_{11}^{(3)}$	$C_{44}^{(3)}$	$-11T_1$	$T_2+2T_3+2T_4+4T_5$
1.771	0	0.295	0.028	−22,850	−23,019
2.35	3.1	0.263	0.022	−22,731	−22,182
2.5	4.2	0.252	0.016	−22,679	−23,328
3.5	19	0.207	0.010	−21,998	−21,936
4.5	55	0.143	−0.013	−20,554	−19,609

nal component than on the transverse one. These contributions are decreasing with pressure and will even change sign under high pressure. But these contributions are known to be strongly dependent on the angular form of the three body-interaction.[23] The Axilrod-Teller potential that is used here to model the many-body interactions is based on the same angular dependence for the exchange three body contribution as the triple-dipole term. Therefore the assumed angular form can strongly influence the relative corrections to the longitudinal and transverse branches. The calculation can be analyzed in two ways.

(i) The HFDID1 represents adequately the repulsive part of the pair potential for the interatomic distance at 3.1 GPa. The observed disagreement in Fig. 8 with IXS data means that the Axilrod-Teller potential does not adequately represent the exchange three-body interactions, particularly through its angular dependence.

(ii) The HFDID1 is not a good pair potential for the interatomic distance corresponding to 3 GPa. But the exp-6 potential could represent better this repulsive part. As seen in Fig. 8, the many-body corrections then go in the good direction : the longitudinal phonon energies are increased, but the correction is only of the order of 1% whereas 7% would have been needed; the correction is very small for the transverse branch already in good agreement with IXS data.

In conclusion, we cannot fully resolve the discrepancy between calculation and IXS data. We show that the many-body interaction can give measurable corrections on the phonon frequencies already at 3 GPa. A better agreement is obtained if the exp-6 is used as the pair potential. But certainly, the magnitude and even the sign of this correction could depend on the geometric form used for the exchange many-body potential. The determination of a many-body potential that could bring agreement between calculations, EOS and IXS data is beyond the scope of this work. In summary, the analysis indeed shows that IXS is a powerful tool to test the many-body interactions of a system at high pressure.

V. CONCLUSION

Third generation synchrotron sources are continuously offering new possibilities to study matter at high density. It is shown here that single-crystal IXS measurements can now be performed in a diamond anvil cell. Measurements were done at 3.1 and 20 GPa and could be extended to Mbar pressure

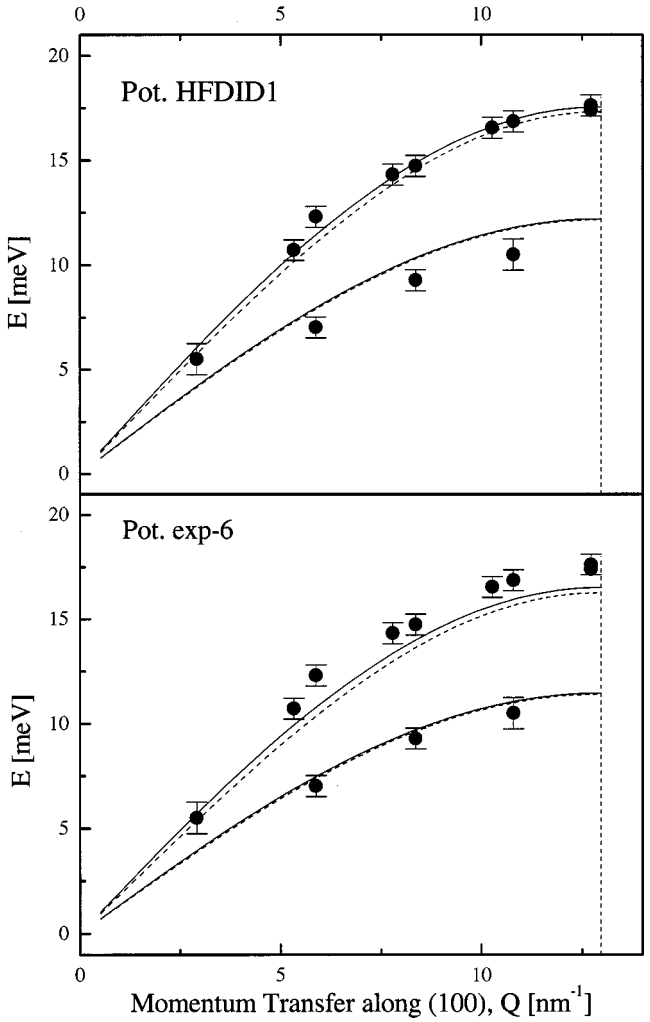

FIG. 8. Effect of nonadditive corrections calculated with the Axilrod-Teller interaction. The symbols are ●: IXS data. Upper, - - -: HFDID1 calculation, —: HFDID1 calculation corrected with Axilrod-Teller interaction. Lower, - - -: exp-6 calculation, —: exp-6 calculation corrected with Axilrod-Teller interaction.

(even with less accumulation time on a heavier element). But, for meaningful data, the quality of the single crystal should be preserved under pressure, for example, by using helium as a pressure transmitting medium. The fine data obtained at 3.1 GPa were analyzed to address the influence of many-body interaction on the dynamical properties. Many-body forces exist in solid argon even at ambient pressure and their influence is a subject of continuous interest. The inclusion of the very small nonadditive exchange contribution was recently found to be necessary to understand the preferred fcc crystal structure at ambient pressure.[21] Many-body contributions on the EOS were shown to become increasingly important under pressure[8] and it is found here that the state-of-the-art argon pair potential is not capable to reproduce the EOS above 10 GPa. It is also shown here that many-body contributions can have a larger influence on the dynamical properties than on the EOS: the IXS transverse data differ by around 10% with the pure pair potential calculations. IXS measurements are important and complemen-

tary to x-ray diffraction to investigate the properties of matter under high pressure. Various applications have been highlighted in the introduction, in particular the possibility to finely test the model of interaction of the system such as embbeded atom potentials, increasingly used now at high pressure. We will just point out here an important possibility for high pressure physics, that is the calibration of an absolute pressure scale. On a single crystal of Ta or Au, which remains cubic at least to above 150 GPa,[24] x-ray scattering will give the volume versus the ruby pressure scale and the IXS will give the bulk modulus versus the ruby pressure scale. The coupling of the two sets of data will give by integration the calibration of the ruby scale versus the absolute pressure.

ACKNOWLEDGMENTS

We acknowledge the European Synchrotron Radiation Facility for provision of synchrotron radiation facilities and we would like to thank the staff of the inelastic x-ray scattering group for assistance. We thank M. Hanfland for the use of ID9 to orient the single crystal. We also thank G. Zérah for continuous interest in this work.

[1] S. Klotz, J.M. Besson, K. Karch, P. Pavone, D. Strauch, and W.G. Marshall, Phys. Rev. Lett. **79**, 1313 (1997).
[2] S. Klotz and M. Braden, Phys. Rev. Lett. **85**, 3209 (2000).
[3] M. Krisch *et al.*, Phys. Rev. B **56**, 8691 (1997).
[4] J. Barker, M.L. Klein, and M. Bobetic, Phys. Rev. B **2**, 4176 (1970).
[5] A. Laio, S. Bernard, G.L. Chiarotti, S. Scandolo, and F. Tossatti, Science **287**, 1027 (2000).
[6] M.I. Baskes, J.S. Welson, and A.F. Wright, Phys. Rev. B **40**, 6085 (1989).
[7] Ronald A. Aziz, J. Chem. Phys. **99**, 4518 (1993).
[8] P. Loubeyre, Phys. Rev. B **37**, 5432 (1988).
[9] R. Le Toullec, J.P. Pinceaux, and P. Loubeyre, High Press. Res. **1**, 77 (1988).
[10] H.K. Mao, J. Xu, and P.M. Bell, J. Phys. G **5**, 4673 (1986).
[11] H.K. Mao, A. Jephcoat, R.J. Hemley, L.W. Finger, C.S. Zha, R.M. Hasen, and D.E. Cox, Science **239**, 1131 (1988).
[12] R. Verbeni, F. Sette, M.H. Krisch, U. Bergmann, B. Gorges, C. Halcoussis, K. Martel, C. Masciovecchio, J.F. Ribois, G. Ruocco, and H. Sinn, J. Synchrotron Radiat. **3**, 62 (1996).
[13] C. Masciovecchio, U. Bergmann, M. Krisch, G. Ruocco, F. Sette, and R. Verbeni, Nucl. Instrum. Methods Phys. Res. B **111**, 181 (1996).
[14] C. Masciovecchio, U. Bergmann, M. Krisch, G. Ruocco, F. Sette, and R. Verbeni, Nucl. Instrum. Methods Phys. Res. B **117**, 339 (1996).
[15] H. Zabel, in *Neutron and Synchrotron Radiation for Condensed Matter Studies*, edited by J. Baruchel *et al.* (Springer Verlag, Paris, 1993), p. 285.
[16] M. Grimsditch, P. Loubeyre, and A. Polian, Phys. Rev. B **33**, 7192 (1986).
[17] M. Ross, H.K. Mao, P.M. Bell, and J.A. Xu, J. Chem. Phys. **85**, 1028 (1986).
[18] R.J. Bell and I.J. Zucker, in *Rare Gas Solids T1*, edited by M.L. Klein and J.A. Venables (Academic Press, New York, 1976), p. 154.
[19] See, for example, D. Frenkel and B. Smit, *Understanding Molecular Simulation* (Academic Press, San Diego, 1996), p. 75.
[20] D.N. Batcheler, M.F. Collins, B.C.G. Haywood, and G.R. Sidey, J. Phys. C **3**, 249 (1970).
[21] V.F. Lotrich and K. Szalewicz, Phys. Rev. Lett. **79**, 1301 (1997).
[22] P. Vinet, J. Ferrante, J.R. Smith, and J.H. Rose, J. Phys. C **19**, 467 (1986).
[23] I.J. Zucker and G.G. Chell, J. Phys. C **2**, 1505 (1968).
[24] H. Cynn and C.S. Yoo, Phys. Rev. B **59**, 8526 (1999).